Marine and Petroleum Geology 73 (2016) 433–444

Contents lists available at ScienceDirect

Marine and Petroleum Geology

journal homepage: www.elsevier.com/locate/marpetgeo

Research paper

Geological models of gas in place of the Longmaxi shale in Southeast Chongqing, South China

Lei Pan [a, b], Xianming Xiao [a], Hui Tian [a, *], Qin Zhou [a], Peng Cheng [a]

[a] State Key Laboratory of Organic Geochemistry, Guangzhou Institute of Geochemistry, Chinese Academy of Sciences, Guangzhou 510640, China
[b] University of Chinese Academy of Sciences, Beijing 100049, China

ARTICLE INFO

Article history:
Received 25 January 2016
Accepted 13 March 2016
Available online 16 March 2016

Keywords:
Longmaxi shale
High-pressure methane adsorption
Gas-in-place
Geological model
Southeast Chongqing

ABSTRACT

Gas-in-place (GIP) is one of the primary controlling factors in shale gas production, but studies examining GIP have been lacking for the Lower Silurian Longmaxi shale in South China. In the present study, a suite of Longmaxi shale samples was collected from an exploratory well in Southeast Chongqing, South China, and the adsorption parameters were fitted using a supercritical Dubinin-Radushkevich (SDR) model based on the high-pressure methane adsorption experiment data for the samples. The results show that the adsorbed phase density and the adsorbed gas capacity of the samples have a positive correlation with the content of total organic carbon (TOC) but a negative correlation with temperature. Combined with the geological characteristics of the Longmaxi shale in Southeast Chongqing, GIP models were constructed under three different fluid pressure conditions. The absolute adsorbed amount of the samples increases and later decreases with increasing depth with a maximum corresponding to depths between 800 and 1200 m. The fluid pressure coefficient has no obvious effect on the absolute adsorbed amount when burial depth is over 2000 m but controls the free gas content. Overpressure primarily increases the free gas content and thus increases the total gas content. The free gas content of the Longmaxi shale in the Pengshui Block is reduced to 47%–58% of that in the Fuling Block, which is the main reason for its low gas production. Further exploration of the Longmaxi Formation should be expanded to deeper burial shales in the eastern area of Southeast Chongqing.

© 2016 Elsevier Ltd. All rights reserved.

1. Introduction

The organic-rich Lower Silurian Longmaxi shale in Southeast Chongqing has become a hot target for shale gas exploration and development in South China for it is commercially producing shale gas at moderate depths, mainly of 1000–4000 m (Guo and Zhang, 2014; Zhou, 2013). High gas production from the Longmaxi shale has been achieved at the Jiaoshiba area in the Fuling Block within the Sichuan Basin, making it the second commercial shale gas field outside North America (Guo and Liu, 2013; Li et al., 2014). The cumulative production reached 12.24 × 10^8 m^3 by the end of 2014 (Liu, 2015). However, exploration of the Lonamaxi shale in the eastern area of Southeast Chongqing (outside the present day Sichuan Basin) has not made substantial progress, and all tested wells have a low gas yield. For example, the initial production of Well PY1 and Well QY1 from the Pengshui Block is approximately 2.0 × 10^4 m^3/d and 0.48–0.84 × 10^4 m^3/d, respectively (Guo et al., 2014; Guo and Zhang, 2014). The Longmaxi shale system in the Fuling Block is overpressured with a pressure coefficient of approximately 1.5, whereas the system has a hydrostatic pressure gradient with a pressure coefficient of approximately 1.0 in the eastern area of Southeast Chongqing (Hu et al., 2014). It is believed that the difference of fluid pressure coefficients is the main reason for the different gas production in the two blocks (Hu et al., 2014). Currently, it is difficult to evaluate the gas potential of the Longmaxi shale in Southeast Chongqing, especially in its eastern area, due to the lack of studies on GIP (Zhang et al., 2013).

Shale gas is stored mainly as free gas and adsorbed gas, and dissolved gas can be neglected for overmature shales where liquid hydrocarbons are only in trace amount (Curtis, 2002; Montgomery et al., 2005; Jarvie et al., 2007; Jarvie, 2012; Ambrose et al., 2012). Therefore, free and adsorbed gas contents are crucial for the evaluation of GIP. Free gas in shale is conventionally calculated using effective porosity, which is defined as total porosity minus the volume occupied by water (Bustin et al., 2009; Zhang et al., 2012a;

* Corresponding author. 511#, Kehua Road, Tianhe District, Guangzhou City, Guangdong Province, 510640, China.
E-mail address: tianhui@gig.ac.cn (H. Tian).

http://dx.doi.org/10.1016/j.marpetgeo.2016.03.018
0264-8172/© 2016 Elsevier Ltd. All rights reserved.

Zhou, 2014), and the adsorbed gas content is represented by absolute adsorbed amount (Zhang et al., 2012b). This method, however, may exaggerate gas capacity because the volume occupied by adsorbed gas is doubly counted in the free gas model. Ambrose et al. (2012) reported that the difference in free gas content calculated with and without considering the adsorbed phase volume can reach 15.4–32.9% under various geological conditions.

The isothermal adsorption experiment of high-pressure methane is a common method to evaluate adsorption capacity of shale (Chalmers and Bustin, 2007; Zhang et al., 2012b; Wang et al., 2013b). While a single isotherm of methane adsorption provides some basic information on methane adsorption (Ross and Bustin, 2007, 2009; Chalmers and Bustin, 2008; Weniger et al., 2010; Chareonsuppanimit et al., 2012; Gasparik et al., 2012), multiple isotherms at a range of temperatures are quite necessary to simulate methane adsorption with depth under geological conditions (Zhang et al., 2012b; Gensterblum et al., 2013; Rexer et al., 2013; Gasparik et al., 2014a; Ji et al., 2014; Bruns et al., 2016).

The geochemical characteristics, pore structure and reservoir physical properties of the Longmaxi shale in South China have been widely reported recently (Liang et al., 2012; Huang et al., 2012; Tian et al., 2013, 2015; Wang et al., 2013a); however, there are only a few papers related to the isothermal methane adsorption of the Longmaxi shale (e.g., Wu et al., 2012; Shi et al., 2015). These adsorption experiments were designed based on shales with different TOC contents at a single temperature (e.g., 30 °C or 60 °C) and at a maximum pressure of 12–15 MPa. These temperature and pressure are far lower in comparison to the current burial depth of the Longmaxi shale in South China, corresponding a geological temperature and a fluid pressure up to approximately 150 °C and 60 MPa, respectively (Tan et al., 2015). Thus, it is very important to conduct methane adsorption experiments at higher temperatures and pressures for an objective evaluation of the GIP of the Longmaxi shale. In the present study, high-pressure methane adsorption experiments on the Longmaxi shale samples collected from one exploratory well in Southeast Chongqing were performed under temperature up to 150 °C and pressure up to 35 MPa, and geological models of GIP were constructed by a combination of the adsorption parameters and the specific geological model in Southeast Chongqing. The primary objective is to investigate gas content of a shale with depth and to provide a scientific basis for a further evaluation of gas potentials of the Longmaxi shale in this area.

2. Geological setting

The Southeast Chongqing mainly includes Fuling, Wulong, Pengshui and Shizhu areas and belongs to the Chuandong Fold Belt (Tian et al., 2013). It is divided into two parts by the Qiyueshan Fault (Fig. 1). The west part belongs to the eastern margin of the Sichuan Basin and is characterized by gentle folds with outcrops of Jurassic–Triassic strata, whereas in the eastern part, fractures and intensively deformed folds are developed to expose Triassic–Silurian strata (Nie et al., 2009; Guo and Liu, 2013; Guo, 2014). The tectonic and sedimentary evolution of Southeast Chongqing is similar to that of the Sichuan Basin, including largely five stages: Early Paleozoic marine deposition with a thickness of 2500–3500 m; an uplift and erosion stage from the Devonian to the Carboniferous with an eroded thickness of 500–1000 m; alternating marine and terrestrial deposition from the Permian to the Middle Triassic with a thickness of 2000–3000 m; terrestrial deposition from the Late Triassic to the Early Cretaceous with a thickness of 3000–4000 m; and tectonic deformation and uplifting during the Late Cretaceous through the Cenozoic with an eroded thickness of 3000–6000 m (Nie et al., 2012; Wang, 2012; Guo and Liu, 2013). The Upper Paleozoic and its overlying strata were denuded in some tectonic uplifts, with outcrops of Cambrian or Silurian strata (Xie et al., 2013).

Black shales are present in both the Lower Cambrian Niutitang and the Lower Silurian Longmaxi formations in Southeast Chongqing (called the Niutitang shale and the Longmaxi shale, respectively) with current burial depths of 3000–7000 m and 1000–5000 m, respectively (Zhang et al., 2008; Han et al., 2013; Xing et al., 2014; Tan et al., 2015). The thickness of the Niutitang shale generally ranges from 60 to 180 m with a TOC content of 3–6% and an EqRo of 3.0–4.0% (Xie et al., 2013; Xing et al., 2014). The thickness of the Longmaxi shale ranges from 50 to 100 m with a TOC content of 2–4% and an EqRo of 2.5–3.0% (Li et al., 2012; Han et al., 2013). Cao et al. (2014) reported that the average porosity and permeability of the Niutitang shale from wells YuKe 1 and YouKe 1 are 1.2% and 8.0×10^{-3} mD, respectively. Sun et al. (2014) reported that the average porosity and permeability of the Longmaxi shale are 3.7% and 29.8×10^{-3} mD, respectively. The Longmaxi shale has become the main target of shale gas extraction in Southeast Chongqing because it has more favorable geological conditions than the Niutitang shale for commercial shale gas development (Han et al., 2013; Tan et al., 2015).

3. Samples and methods

3.1. Samples and experiments

The Longmaxi shale samples for the present study were collected from an exploratory well (PY1) at an interval of 2122–2150 m (Fig. 1); and their geochemical and pore structural characteristics were previously reported by Tian et al. (2013). Briefly, their TOC values are in the range of 1.01–3.98% with EqRo value ranges from 2.84% to 3.05% (Table 1). These samples are rich in clay minerals, ranging from 38.5% to 52.5%, and quartz and feldspar content in the range of 21.6–30.5% and 8.0–29.3%, respectively. The total porosity ranges between 2.6% and 4.76%, and the BET surface area ranges between 5.06 and 19.32 m^2/g (Table 1).

Each sample (approximately 60 g) was dried at 60 °C in a vacuum for 24 h and then was crushed and sieved for a 40–80 mesh (380–180 μm) size fraction. The selected samples were dried again at 110 °C in a vacuum for 24 h to remove free water before high-pressure methane adsorption analysis.

The high-pressure methane adsorption measurements were conducted using the magnetic suspension balance ISOSORP-HP Static II (Rubotherm GmbH, Germany). The precision of the magnetic suspension balance is 0.01 mg, and the maximum values of pressure and temperature are 35 MPa and 200 °C, respectively. The temperature of the sample container is controlled using a heating oil bath cycle with an accuracy of 0.01 °C. The mass change of a sample exposed to the sorptive gas (methane in this study) at a definite temperature and variable pressures is directly measured by the equipment, and the excess adsorption amount is then calculated by the blank and buoyancy corrections at the given temperature (Gasparik et al., 2014b). For all samples, the experimental temperature was 60 °C. Five extra temperature points (40, 80, 100, 120, and 150 °C) were measured for Sample 8 to construct the relationship between adsorbed gas capacity and burial depth. The detailed experimental procedures for the magnetic suspension balance equipment have been well documented in previous publications (Giovanni et al., 2001; Ottiger et al., 2008; Pini et al., 2006, 2010; Gasparik et al., 2014b).

3.2. Calculation of adsorption gas

3.2.1. Excess adsorption and absolute adsorption

According to the Gibbs adsorption model (Murata et al., 2001,

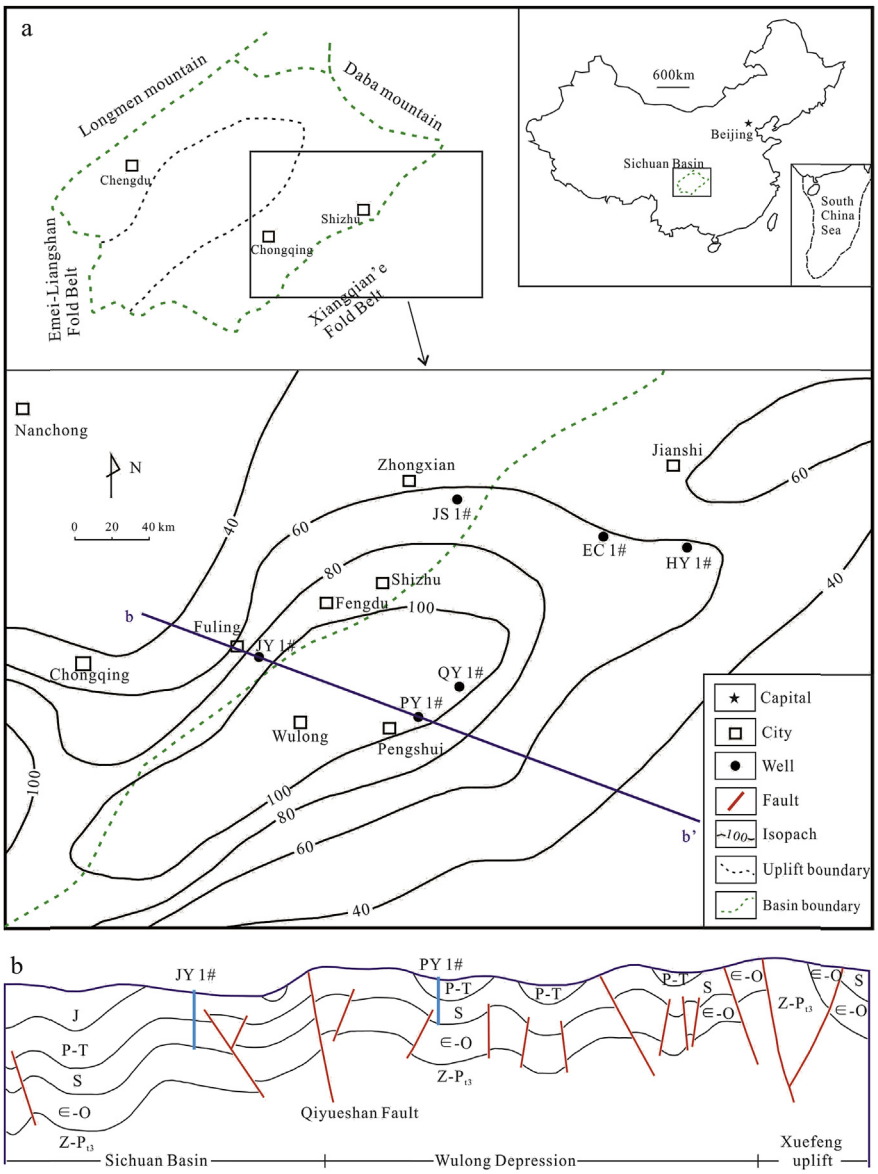

Fig. 1. A sketch map showing the thickness of the Lower Silurian organic-rich shale (the Longmaxi shale) in the Southeast Chongqing (a), and a geological crossection through the Pengshui and Fuling shale gas blocks (b) (modified from Liu et al., 2009; Hu et al., 2014; Zhai, 2014).

Table 1
TOC, equivalent vitrinite reflectance (EqRo), porosity, BET surface area and mineralogical composition of the studied samples (data from Tian et al., 2013).

Sample	Depth (m)	TOC (wt.%)	EqRo (%)	Porosity (%)	S_{BET} (m^2/g)	Mineralogical composition relative percent (%)			
						Quartz	Feldpar	Clays[a]	Other[b]
Sample 1	2122.5	1.42	nd[c]	3.04	9.31	22.7	29.3	45.1	2.9
Sample 2	2126.8	1.01	nd	2.76	5.06	24.9	17.6	44.9	12.6
Sample 3	2131.3	1.56	2.87	2.6	7.86	21.6	27.3	44.3	6.8
Sample 5	2136.8	2.62	2.84	3.14	12.94	27.0	17.4	38.5	17.1
Sample 6	2140.8	3.47	nd	4.76	16.51	29.3	8.0	52.5	10.2
Sample 7	2144.8	3.41	3.05	4.01	15.91	30.5	10.2	49.2	10.1
Sample 8	2149.7	3.98	2.94	4.74	19.32	30.1	10.6	52.5	6.8

S_{BET}: BET surface area.
[a] Clays = illite + montmorillonite + chlorite.
[b] Others = Carbonate + Pyrite.
[c] nd = No data.

2002; Bae and Bhatia, 2006; Ottiger et al., 2006; Pini et al., 2010), excess adsorption is related to absolute adsorption through the following equation:

$$n_{\mathrm{ex}} = n_{ab} \cdot \left(1 - \frac{\rho_b}{\rho_{ad}}\right) \tag{1}$$

where n_{ex} is the excess adsorption, n_{ab} is the absolute adsorption, ρ_{ad} is the adsorbed phase density, and ρ_b is the bulk gas phase density.

Both the Langmuir and supercritical Dubinin-Radushkevich (SDR) models are commonly used to characterize the adsorption properties of shale (Sakurovs et al., 2007; Gensterblum et al., 2009, 2014; Rexer et al., 2013). The Langmuir model is based on assumptions of homogeneous pore structure, monolayer adsorption, and lack of interaction between gas molecules (Langmuir, 1918; Ambrose et al., 2012; Zhang et al., 2012b; Gensterblum et al., 2014). This model has been improved to be a classical adsorption model and is widely used to investigate the adsorption characteristics of coal and shale (Sakurovs et al., 2007; Pini et al., 2010; Gensterblum et al., 2009; Gasparik et al., 2012, 2014a). The SDR model was developed on the basis of the classical Dubinin-Radushkevich (DR) equation, which was originally established for low-pressure subcritical adsorption (Gregg and Sing, 1982; Dubinin, 1989; Clarkson et al., 1997). The DR equation cannot be used directly to model supercritical adsorption of gas in reservoir conditions because the saturated vapor pressure cannot be defined. Therefore, Sakurovs et al. (2007) proposed that the relative pressure in the original DR equation could be replaced by the ratio of bulk density to adsorbed phase density, thus the modified DR (i.e., SDR) model can be used to describe high-pressure methane adsorption under supercritical conditions. The SDR model takes the following form (e.g., Rexer et al., 2013):

$$n_{\mathrm{ex}} = n_0 \cdot \exp\left\{ -D \cdot \left(ln\left(\frac{\rho_{ad}}{\rho_b}\right) \cdot RT \right)^2 \right\} \cdot \left(1 - \frac{\rho_b}{\rho_{ad}}\right) \tag{2}$$

where n_0 is the maximum absolute adsorption, R is the ideal gas constant, T is the absolute temperature (K), and D is an interaction constant related to pore structure and equal to $1/(\beta E_0)^2$ where β and E_0 are characteristic parameters of the adsorbent (White et al., 2005).

Rexer et al. (2013) made a comparison between the SDR and Langmuir models using the methane adsorption data collected at supercritical conditions and suggested that the former is more reasonable than the later for characterizing methane adsorption on shales because the density of adsorbed methane fitted by the SDR model is less than the liquid density of methane at its boiling point (i.e., 0.424 g/cm^3). Therefore, the SDR model is used to characterize methane adsorption under supercritical condition in the present study.

An assumption is needed that the adsorbed phase density of methane would remain constant with increasing pressure when the free parameters (n_0, D and ρ_{ad}) are fitted in Eq. (2) by the SDR model. This assumption has been confirmed by experimental data (Murata et al., 2001; Krooss et al., 2002; Sudibandriyo et al., 2003; Ottiger et al., 2006; Bae and Bhatia, 2006; Pini et al., 2006, 2010; Chareonsuppanimit et al., 2012; Rexer et al., 2013).

3.2.2. Excess adsorption model

The calculation formula of the excess amount of adsorbed methane at specific geological conditions can be deduced using the SDR model. With the burial depth given as H (m), the geothermal gradient as T_g (K/m), the surface temperature as T_o (K) and the pressure coefficient as y, the formula can be expressed by:

$$n_{ex}^{H} = n_o^{H} \cdot \exp\left\{ -D \cdot \left(ln\left(\frac{\rho_{ad}^{H}}{\rho_b^{(H,T,y)}}\right) \cdot R \cdot (T_o + H \cdot T_g) \right)^2 \right\} \cdot \left(1 - \frac{\rho_b^{(H,T,y)}}{\rho_{ad}^{H}}\right) \tag{3}$$

where n_{ex}^{H}, n_o^{H} and ρ_{ad}^{H} are the excess adsorption, the maximum absolute adsorption and the adsorbed phase density at a burial depth H, respectively, and $\rho_b^{(H,T,y)}$ is the bulk gas density at corresponding temperature and pressure (the pressure and temperature equals $0.01 \cdot y \cdot H$ MPa and $T_o + H \cdot T_g$ K, respectively).

3.3. Calculation of total gas, absolute adsorbed gas and free gas

According to the Gibbs adsorption theory, the total gas, absolute adsorbed gas and free gas at specific geological conditions can be calculated using the following equations, respectively:

$$n_{total}^{H} = n_{ex}^{H} + \frac{\varphi \cdot (1 - S_w)}{\rho_{apparent}} \cdot \frac{\rho_b^{(H,T,y)}}{\rho_b^{\mathrm{STP}}} \tag{4}$$

$$n_{ab}^{H} = \frac{n_{ex}^{H} \cdot \rho_{ad}^{H}}{\rho_{ad}^{H} - \rho_b^{(H,T,y)}} \tag{5}$$

$$n_{free}^{H} = n_{total}^{H} - n_{ab}^{H} \tag{6}$$

where S_w is water saturation, φ is porosity, ρ_{apparent} is the apparent density of a shale, ρ_b^{STP} is the density of methane at standard temperature and pressure conditions (0 °C and 0.1 MPa), and n_{total}^{H}, n_{ab}^{H} and n_{free}^{H} are the total gas, absolute adsorbed gas and free gas at a burial depth of H, respectively.

In the above equations (3)–(6), H, T_g, T_o and S_w are the given geological parameters, φ and $\rho_{apparent}$ are basic physical parameters of shale which can be obtained by corresponding experiments (Tian et al., 2013), n_o^{H}, ρ_{ad}^{H} and D are adsorption parameters which can be fitted by the SDR model (Sakurovs et al., 2007; Rexer et al., 2013), and $\rho_b^{(H,T,y)}$ can be calculated by the PVT equation (Zhou et al., 2014b).

It is should be noticed that the moisture in shales could reduce their capacity of methane adsorption (Chalmers and Bustin, 2008; Busch and Gensterblum, 2011; Gasparik et al., 2014a; Gensterblum et al., 2014), therefore the geological extrapolation based on the dry adsorption data should be regarded as a maximum scenario (Bruns et al., 2016).

4. Results and discussions

4.1. Isothermal adsorption curve and data fitting

The excess adsorbed amount of the samples was directly measured by the magnetic suspension gravimetric method, and the absolute adsorbed amount was calculated through adsorption parameters (Table 2) fitted by the SDR model (Sakurovs et al., 2007; Rexer et al., 2013). As revealed in Figs. 2 and 3, the SDR model has a perfect fit of the measured data, with fitting coefficients as high as 0.99. The excess and absolute adsorbed amounts show completely different trends with increasing pressure (Figs. 2 and 3). The excess amount increases rapidly at first with pressure and reaches a maximum at 9–10 MPa, and then begins to decrease with

Table 2
Adsorption parameters of the studied samples fitted by SDR model (60 °C).

Sample	Maximum excess absorbed capacity and corresponding pressure		Parameters fitted by the SDR model		
	n_{ex}^{max} (cm^3/g)[a]	Pressure (MPa)	N_o (cm^3/g)[a]	D (mol^2 KJ^{-2})	ρ_{ad} (g/cm^3)
Sample 1	0.93	~9	1.466	0.0125	0.224
Sample 2	0.59	~8	0.939	0.0135	0.218
Sample 3	0.96	~9	1.488	0.0119	0.242
Sample 5	1.49	~10	2.236	0.0100	0.276
Sample 6	1.74	~10	2.625	0.0098	0.285
Sample 7	1.68	~10	2.567	0.0108	0.28
Sample 8	1.81	~10	2.699	0.0092	0.291

n_{ex}^{max}: the maximum excess adsorption capacity; N_o: the maximum absolute adsorption capacity; ρ_{ad}: the density of adsorbed methane; D: the parameter of pore structure.
[a] 1 mmol/g = 16 mg/g = 22.4 cm^3/g @STP.

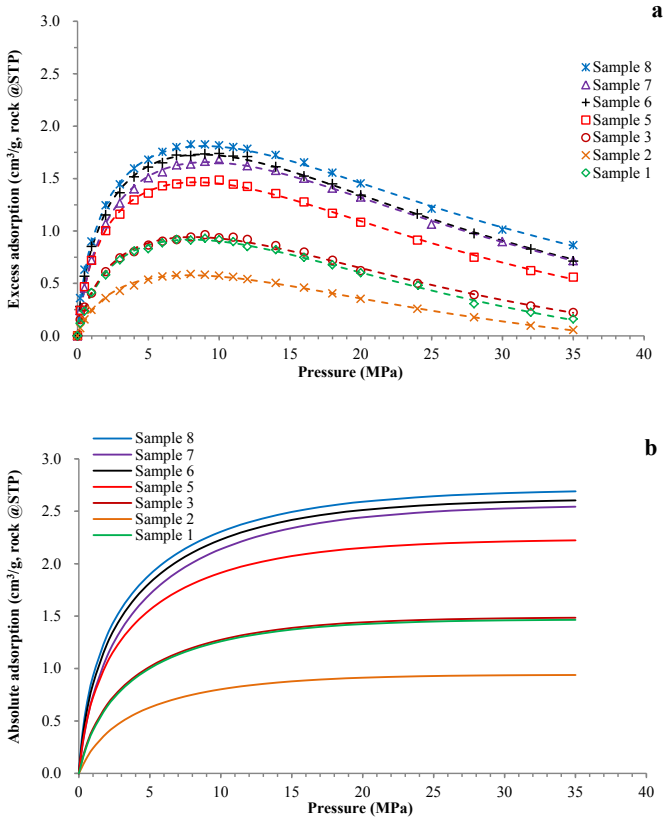

Fig. 2. Measured and fitted methane excess adsorption isotherms (a) and calculated absolute adsorption isotherms using the SDR model (b) for the studied samples at 60 °C.

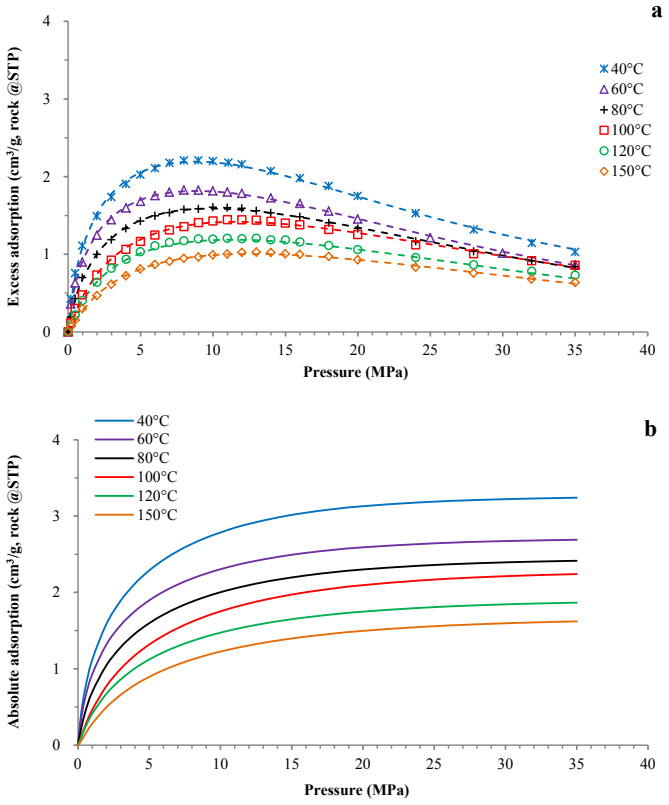

Fig. 3. Measured and fitted methane excess adsorption isotherms of Sample 8 (TOC = 3.98%) at different temperatures (40–150 °C) (a) and their absolute adsorption isotherms calculated by the SDR model (b).

further increasing pressure. The shape of the absolute adsorption curve is similar to the Type I adsorption curve defined by IUPAC (Rouquerol et al., 1994), with a rapid increase when pressure is less than 9–10 MPa (i.e., the pressure of the maximum excess adsorbed amount) and a slow increase with a further increasing pressure. If the experimental pressure continues to increase, the excess adsorbed amount would be reduced to zero as the bulk methane density is equal to the adsorbed phase density, which means that there is no measurable excess adsorption. As both the free methane density and the volume of adsorbed methane increase with pressure, their product, i.e., the difference between the absolute and excess adsorbed amounts, also gradually increases with pressure (Figs. 2 and 3).

The adsorption isotherms vary with the TOC content of sample (Fig. 2); the higher the TOC content, the greater the amount adsorbed. Samples with higher TOC contents require higher pressures for the excess adsorption to approach zero (Fig. 4), indicating a positive correlation of density of adsorbed methane with TOC. There is a significant difference in the adsorption curves of Sample 8 obtained at different temperatures (Fig. 3). The excess adsorption decreases with increasing temperature, and the pressure corresponding to the maximum excess adsorption also increases with increasing temperature (Fig. 3). A greater pressure is needed for the excess adsorption to approach zero for the adsorption at a higher temperature. All these characteristics of methane adsorption on our samples are consistent with those of coals and shales reported in the literature (e.g., Bae and Bhatia, 2006; Sakurovs et al., 2007; Pini et al., 2010; Rexer et al., 2013; Gensterblum et al., 2014; Bruns et al., 2016).

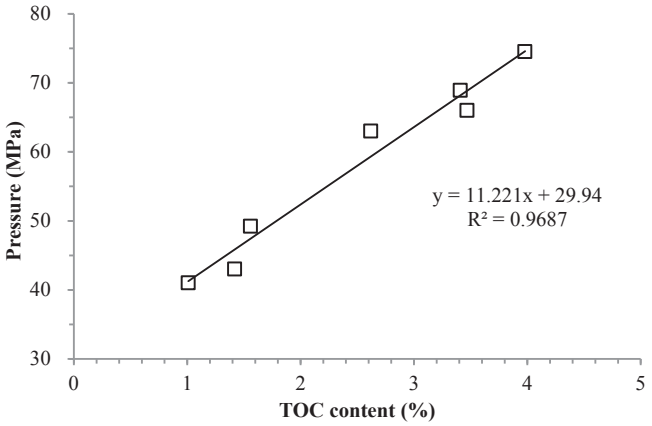

Fig. 4. Plot showing the relationship between the TOC content and the pressure corresponding to a zero excess adsorption at 60 °C.

4.2. Influence of TOC content on adsorption parameters

Both the maximum excess and absolute adsorbed amounts of the samples show a linear positive correlation with TOC content (Fig. 5a, Table 2), implying that the organic matter in shale is the main carrier of the adsorbed methane. The maximum excess and absolute amounts for a sample without organic matter (TOC = 0%), deduced from the regression equations (Fig. 5a), are 0.31 and 0.54 cm^3/g, respectively, indicating that minerals can also contribute a portion of methane adsorption capacity (Ji et al., 2012).

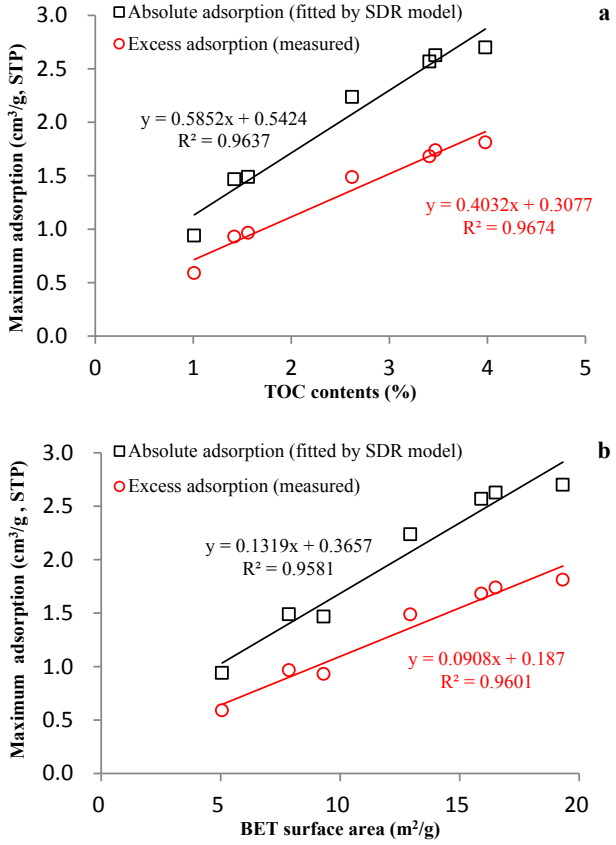

Fig. 5. Plots showing the relationships between the maximum adsorption capacity with the TOC content (a), and the BET surface area (b) for the studied samples at 60 °C.

Strongly positive correlations between the adsorption capacity and the BET surface areas (Fig. 5b, Table 2) imply that the methane adsorption sites are offered not only by micropores but also by the surface areas of mesopores and even macropores (Montgomery et al., 2005; Hill et al., 2007; Ross and Bustin, 2008; Mosher et al., 2013).

The density of methane in adsorbed phase at 60 °C ranges from 0.22 to 0.30 g/cm^3 and is less than the liquid density of methane at its boiling point (0.424 g/cm^3); and a strongly linear positive correlation exists between the adsorbed phase densities and the TOC contents (Fig. 6a; Table 2). Ambrose et al. (2012) also reported that the adsorbed phase density of an Alum Shale sample (TOC = 6.35%, EqRo = 2.26%) was 0.37 g/cm^3, which plots along the regressed linear line in Fig. 6a. The parameter D is adversely related to the pore size of the shale (White et al., 2005; Rexer et al., 2013); and is negatively related to the TOC content (Fig. 6b) because the organic matter usually contains more micropores than the minerals (Ross and Bustin, 2009).

4.3. Influence of temperature on adsorption parameters

The adsorption parameters of Sample 8 under different temperatures are listed in Table 3. It is clear to see the density of adsorbed methane, as well as its maximum excess and absolute adsorption capacity, all decrease with increasing temperature (Table 3; Fig. 7); and they all show strong linear correlations with the reciprocal of absolute temperature ($0.95 < R^2 < 0.98$) (Fig. 7),

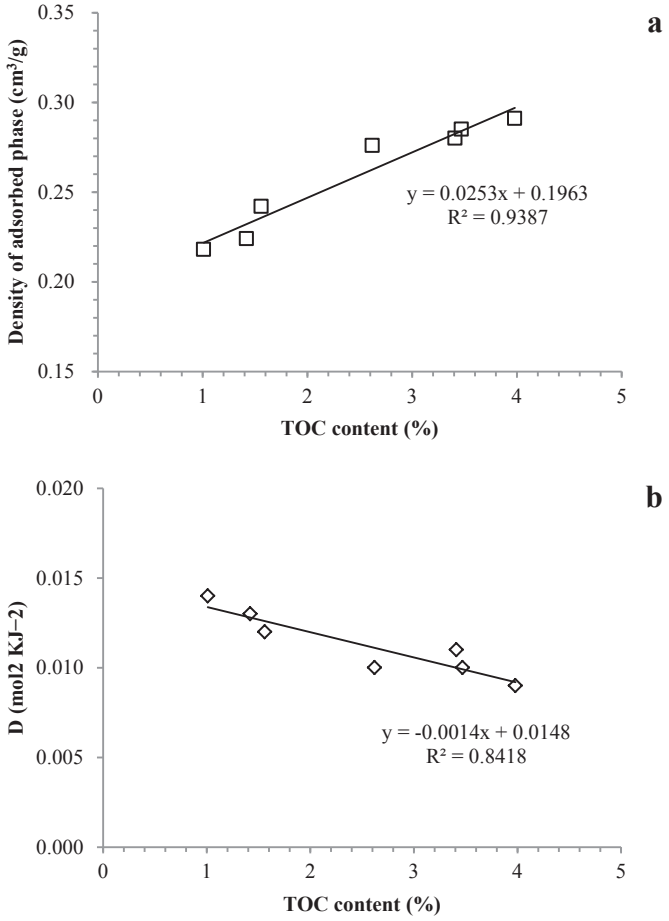

Fig. 6. Plots showing the relationships between the TOC and the density of adsorbed methane (a), and the pore structure parameter D (b) for the studied samples at 60 °C.

Table 3
Adsorption parameters of sample 8 fitted by SDR model (40–150 °C).

Temperature (°C)	1/Temperature (1/K)	No (cm^3/g)[a]	D	ρ_{ad} (g/cm^3)	n_{ex}^{max} (cm^3/g)[a]
40	0.003195	3.185	0.0092	0.324	2.212
60	0.003003	2.718		0.291	1.792
80	0.002833	2.487		0.290	1.652
100	0.002681	2.361		0.275	1.512
120	0.002545	1.900		0.259	1.187
150	0.002364	1.664		0.242	1.036

[a] 1 mmol/g = 16 mg/g = 22.4 cm^3/g @STP.

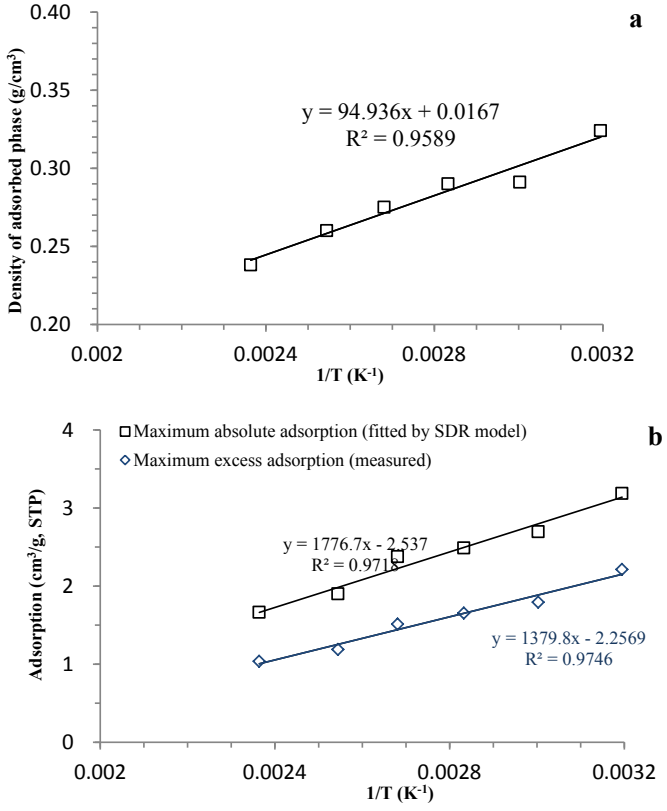

Fig. 7. Plots showing the relationship between the reciprocal of temperature and the density of adsorbed methane (a), the maximum excess and absolute adsorption capacity (b) for Sample 8 (TOC = 3.98%).

which is similar to the Alum shale sample reported by Rexer et al. (2013). Nevertheless, these values of the Alum shale are significantly higher than those of the Longmaxi shale sample at the same temperature (e.g., the adsorbed phase density is 0.21–0.46 g/cm^3, the maximum excess amount is 1.52–3.40 cm^3/g, and the maximum absolute amount is 2.46–4.91 cm^3/g for the Alum shale in the temperature range of 35–150 °C). This is because the Alum shale has a much higher TOC content (6.35%) than the studied samples and that the TOC content is a main factor controlling the capacity of methane adsorption on shales (Chalmers and Bustin, 2008; Ross and Bustin, 2009).

4.4. Geological parameters

The current geothermal gradient in Southeast Chongqing ranges between 21 and 23 °C/km (Yuan et al., 2006). Zhou et al. (2014a) reported that the measured temperature of the Longmaxi shale reservoir based on a horizontal well in the Fuling Block is 64 °C at a depth of 2300 m, which gives a geothermal gradient of 22 °C/km with a surface temperature of 15 °C. The fluid pressure coefficient of the Longmaxi shale system varies greatly in the studied area. It is an overpressure system with a pressure coefficient of 1.5–2.0 within the Sichuan Basin (e.g., the Fuling Block), whereas it is almost a hydrostatic system with a pressure coefficient of approximately 1.0 outside the Sichuan Basin (e.g., the Pengshui Block) (Fig. 1; Hu et al., 2014). The water saturation in shale from productive wells in North America mainly ranges between 12% and 35% (Frantz et al., 2005; Cusack et al., 2010; Mullen, 2010; Hammes et al., 2011; Jarvie, 2012). According to the data of Liu and Wang (2013), the water saturation of the Longmaxi shale in the Southern Sichuan Basin is between 20% and 45% with an average value of approximately 30%. The water saturation of the Longmaxi shale is most related to the fluid pressure coefficient in South China, but there are also obvious differences in different blocks. For example, the water saturation of the Wei 201 and Ning 201 wells in the Weiyuan-Changning Blocks is in the range of 30–45%, and the JY4 well in the Fuling Block is in the range of 9.75%–28.45% with an average of approximately 20% (Liu and Wang, 2013; Wei and Wei, 2014). Based on the sedimentary and tectonic evolution in Southeast Chongqing, the Longmaxi Shale reached a maximum depth of 7000–8000 m in the early Cretaceous age and then suffered from an intensive uplift and erosion, with an eroded thickness of 3000–6000 m in most of the studied area (Liu et al., 2009). The present burial depth ranges mainly between 500 and 5000 m (Tan et al., 2015).

Based on the preceding geological setting, the following geological parameters were assigned to calculate the adsorbed gas and GIP of the Longmaxi shale: a geothermal gradient of 22 °C/km, a surface temperature of 15 °C, a water saturation of 20% for the shales with fluid pressure coefficients of 1.5 and 2.0, a water saturation of 30% for the shales with a fluid pressure coefficient of 1.0, and a maximum present day burial depth of 6000 m.

4.5. Geological models of GIP

4.5.1. Excess adsorption models

Using Eq. (3), the assigned geothermal gradient and the experimental parameters of Sample 8 at different temperatures were used to calculate the excess absorption capacity of methane with depth for three different pressure gradients (i.e., fluid pressure coefficients) (Fig. 8). The excess adsorption capacity increases rapidly and then tends to decrease with increasing depth, with a maximum at a depth between 300 and 600 m.

The fluid pressure coefficient has an obvious influence on the excess adsorption capacity. For a shale system with a greater pressure coefficient, there is a greater maximum excess adsorption capacity which decreases faster as the depth crosses the turning point, and the depth corresponding to the zero excess adsorption is also shallower because the density of free methane is larger in an overpressure system than in a hydrostatic system at the same temperatures, thus the disappearance of difference in density between the free and adsorbed methane can occur at a shallower depth. The disappearance depth of excess adsorption is

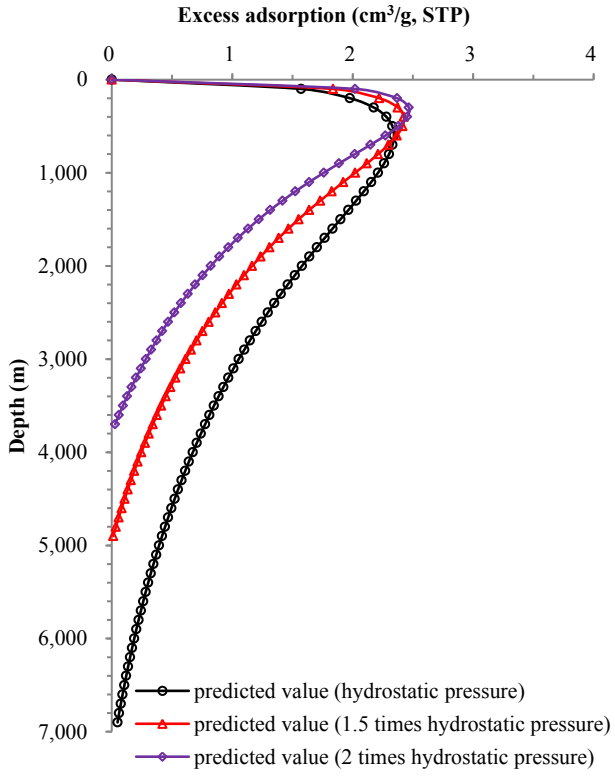

Fig. 8. Plot showing the relationships between the excess adsorption capacity and burial depth for the shale systems with three different fluid pressure coefficients (Sample 8, TOC = 3.98%).

approximately 7000 m with a pressure coefficient of 1.0, shifting upward to 5000 m and 3850 m with a pressure coefficient of 1.5 and 2.0, respectively (Fig. 8).

4.5.2. GIP models

The capacity of absolute adsorbed gas, total gas and free gas for a shale system with various pressure coefficients at different burial depths was calculated using the Equations (4)–(6) based on the excess adsorption model as well as the data of shale porosity and water saturation. The GIP models of the Longmaxi shale systems constructed under three different pressure coefficients (1.0, 1.5 and 2.0) are presented in Fig. 9 and show similar trends with increasing depth: (1) the free gas increases rapidly; (2) the total gas increases rapidly at shallower depth, but increases slowly at deeper depths (>2000 m or so), and (3) the absolute adsorbed gas capacity increases rapidly at first, reaches a maximum at 800–1200 m, and then gradually decreases with further increasing depth, similar to the adsorption model of a high rank coal whose maximum adsorption occurs at approximately 800 m (Hildenbrand et al., 2006).

A greater fluid pressure coefficient can significantly increase the free gas and total gas contents, but its influence on the absolute adsorbed capacity is limited and mainly occurs at shallow burial depths (<2000 m) (Fig. 9). For example, the absorbed gas capacity at a depth of 1200 m is 2.83 cm^3/g, 3.00 cm^3/g and 3.08 cm^3/g with a pressure coefficient of 1.0, 1.5 and 2.0, respectively. The difference in absorbed gas capacity among the three pressure systems decrease with increasing depth and could be ignored at depths greater than 3000 m (Fig. 9). Thus, the fluid pressure coefficient affects the total gas content mainly by increasing the free gas content.

The loss of shale gas as well as its change in stored state during

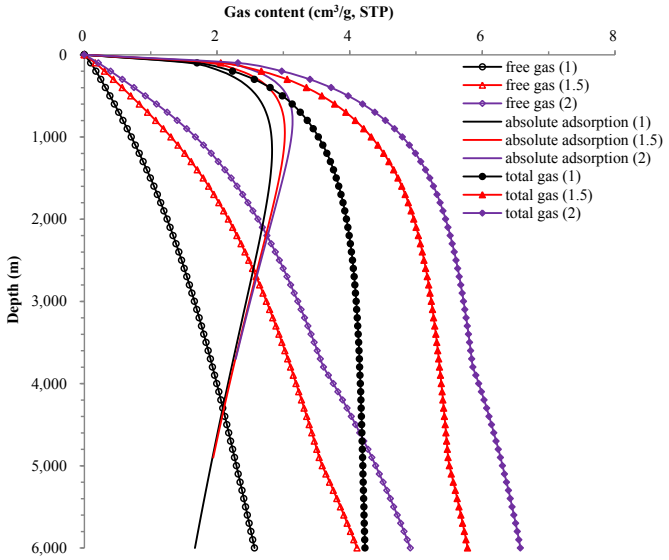

Fig. 9. Geological GIP models of the Longmaxi shale systems under three different fluid pressure systems. This model is based on Sample 8 with a TOC content of 3.98% and a total porosity of 4.76% under a geothermal gradient of 22 °C/km and a surface temperature of 15 °C. The water saturation is 20% for a pressure coefficient of 1.5 or 2.0, and 30% for a pressure coefficient of 1.0. The number in bracket is the pressure coefficient.

uplift and erosion can also be evaluated using the preceding model (Fig. 9). The total gas content only slightly decreases as the burial depth decreases from 6000 to 2000 m, with most of the free gas being converted to the adsorbed gas. The total gas content obviously decreases from 2000 m to 1000 m, with only a portion of the free gas being converted to the adsorbed gas and most of the free gas being lost if the pore volume or fluid pressure coefficient keeps constant. The total gas content rapidly decreases at depths less than 1000 m because of the reduction in the capacity of both free and adsorbed gas. During the entire uplift process, the percentage of the adsorbed gas continually increases due to the reduction in free gas capacity (Fig. 10).

4.5.3. Influence of TOC content on GIP

Based on the adsorption data of the studied samples (Tables 1 and 2) and geological parameters (geothermal gradient and surface temperature), the amounts of the gases versus the TOC content at a current burial depth of 2000 m (approximately 60 °C) were calculated for the Longmaxi shale systems with different pressure coefficients (Fig. 11). With increasing TOC content, the adsorbed and total gas content increases linearly and exponentially, respectively. However, the free gas content has a different pattern; it reaches the smallest level at a TOC content of approximately 2.0% and increases significantly with increasing or decreasing TOC content (>2% or <2%). This complex pattern is caused by the fact that the free gas content in the present study has been corrected by the volume of adsorbed methane whose value varies among samples in terms of the absolute methane adsorption capacity and the density of adsorbed methane. As far as the pressure coefficient is concerned, a greater pressure coefficient leads to greater free gas content, thus increasing the total gas (Guo and Liu, 2013; Hu et al., 2014) (Fig. 11). The ratio of free gas to adsorbed gas is mainly controlled by pressure coefficient and TOC content for a shale system over its TOC range if the water saturation is constant.

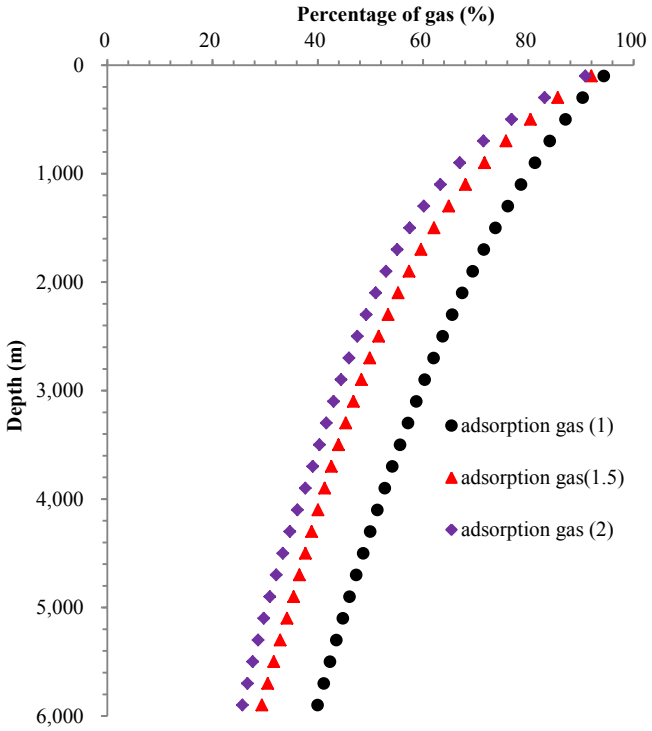

Fig. 10. Plot showing variations of percentage of absorbed gas (absorbed gas/total gas) versus depth. This plot is based on Sample 8 with a TOC content of 3.98% and a total porosity of 4.76% under a geothermal gradient of 22 °C/km and a surface temperature of 15 °C. The water saturation is 20% for a pressure coefficient of 1.5 or 2.0, and 30% for a pressure coefficient of 1.0. The number in bracket is the pressure coefficient.

4.6. Geological application

The difference of shale gas production between the Fuling and Pengshui blocks in Southeast Chongqing can be partly explained by the GIP models proposed in the present study. Geochemical characteristics and gas content data of the Longmaxi shale from the two blocks are listed in Table 4. Although the shales from the two blocks have similar geochemical characteristics and burial depth (Wang, 2014; Yang et al., 2014; Guo, 2014), there are obvious differences in their preservation conditions owing to different structural positions (Wei and Wei, 2014; Guo et al., 2014; Guo, 2014; Gan et al., 2015). The shale system in the Fuling Block is overpressurized with a pressure coefficient of approximately 1.5, while the shale system in the Pengshui Block is a hydrostatic pressure system with a pressure coefficient of approximately 1.0. The adsorbed gas contents of the two shale systems are quite similar, but their free gas contents are significantly different. For example, the adsorbed gas contents of the shales with TOC contents of 2%–4% are 1.8–2.7 cm^3/g in the Fuling Block and1.8–2.6 cm^3/g in the Pengshui Block, and their free gas contents are 0.99–2.34 cm^3/g and 0.47–1.35 cm^3/g, respectively. The free gas content of the Pengshui Block is only approximately 47–58% of that of the Fuling Block. The lower free gas content is the direct reason for the low gas production in the Pengshui Block.

The intensity of tectonic reformation controls the preservation conditions of shale gas and consequently affects the fluid pressure coefficient. The GIP and its free gas percentage of a shale is also controlled by burial depth. According to the geological models in Fig. 9, the free gas content of the Longmaxi shale at 4500 m in the Pengshui Block is equal to that at 2000 m in the Fuling Block. Therefore, overpressured reservoirs with a better preservation condition in more deeply buried shale are favorable exploration

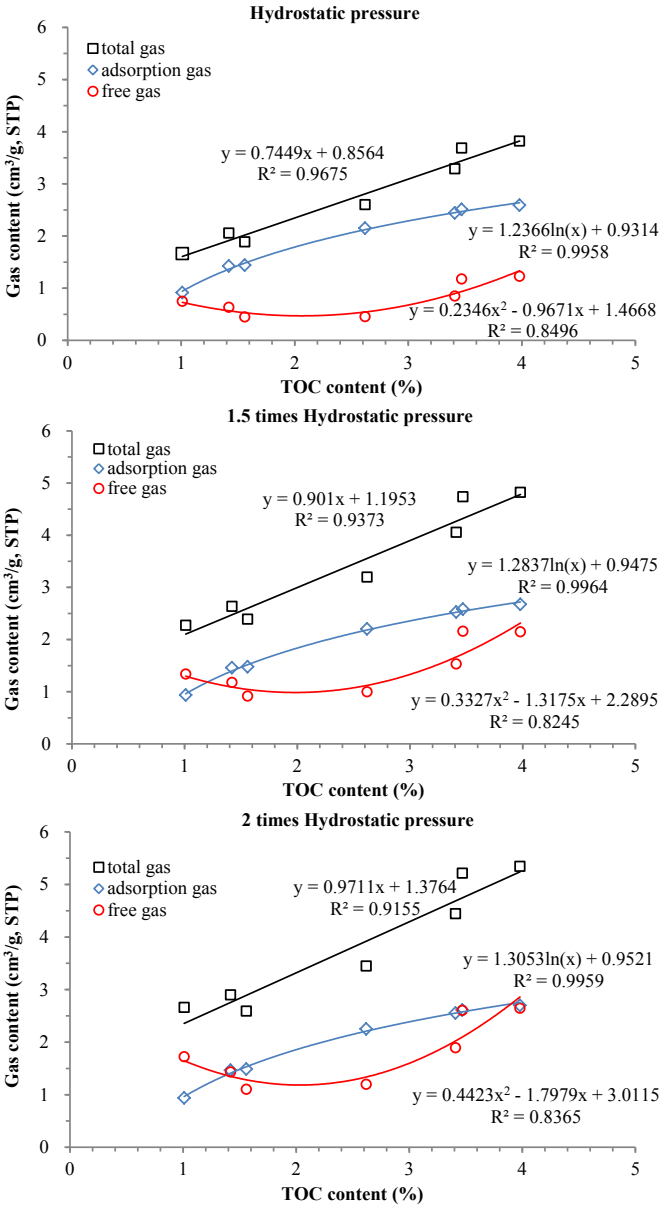

Fig. 11. Plots showing the relationships of the TOC content and the GIP of shales with different pressure coefficients based on the adsorption and porosity data of the studied samples. The reservoir temperature is 60 °C, and the water saturation is 20% for the reservoir with a pressure coefficient of 1.5 or 2.0, and 30% for the reservoir with a pressure coefficient of 1.0.

targets of the Longmaxi shale in Southeast Chongqing, especially in its eastern area.

5. Conclusions

Based on the experimental results of high-pressure methane adsorption of the Longmaxi shale samples from Southeast Chongqing, the following conclusions have been drawn from an investigation of the relationships of adsorption parameters with TOC contents or temperatures and the construction of geological models of GIP under specific geological conditions:

(1) The density of adsorbed methane is mainly constrained by TOC content and adsorption temperature. It is positively related to TOC, but adversely to temperature.

Table 4
Geological and geochemical characteristics, and estimated GIPs of the Longmaxi shale in the Fuling and Pengshui blocks in Southeast Chongqing.

Block		Fuling (well JY1)	Pengshui (well PY1)
Block position		Western area of Southeast Chongqing (within Sichuan Basin)	Eastern area of Southeast Chongqing (outside Sichuan Basin)
Geological and geochemical parameters of the Longmaxi shale	Depth (m)	2377–2416 (Wang, 2014)	2300–2396 m (Yang et al., 2014)
	Thickness (m)	38 (Wang, 2014)	40 (Yang et al., 2014)
	Average TOC (%)	3.5 (Guo, 2014)	3.5 (Yang et al., 2014)
	Average Porosity (%)	4.61 (Guo, 2014)	4.4–4.9 (Yang et al., 2014)
	Average Water saturation (%)	20 (Wei and Wei, 2014)	30 (Gan, 2015)
	Pressure coefficient	1.45–1.55 (Guo, 2014; Guo et al., 2014)	0.9–1.0 (Guo, 2015)
GIP data of the Lonamgxi shale	Total gas (m^3/t)	2.27–4.82	1.66–3.82
	Free gas (m^3/t)	0.91–2.16	0.45–1.23
	Adsorption gas (m^3/t)	0.94–2.67	0.92–2.59
	Free gas/adsorption gas	0.45–1.43	0.21–0.82

(2) With increasing depth, both the free gas and total gas content increases, but the excess and absolute adsorbed capacity show at first a rapid increase and then an obvious decrease with a maximum value occurring at depths of 300–600 m and 800–1200 m, respectively.
(3) The fluid pressure coefficient has a significant effect on excess adsorbed capacity but only has a minor influence on absolute adsorbed capacity. The depth at which the excess absorbed capacity disappears becomes shallower for a shale system with a greater pressure coefficient. Overpressure increases the GIP content mainly through increasing the free gas content of shale.
(4) The free gas content of the Longmaxi shale in Pengshui Block is only approximately 47–58% of that of the Fuling Block, which is the main reason for its low production. The exploration of the Longmaxi shale gas in the eastern area of Southeast Chongqing should focus on deeper depths.

Acknowledgments

This study was supported by a special program of Chinese Academy of Science (XDB10040300), the National Key Basic Research Program of China (973 Program: 2012CB214705), and the National Natural Science Foundation of China (41522302; 41321002). This is contribution No.IS-2208 from GIGCAS.

References

Ambrose, R.J., Hartman, R.C., Diaz-Campos, M., Akkutlu, I.Y., Songdergeld, C.H., 2012. Shale gas-in-place calculations part I: new pore-scale considerations. SPE J. 17, 219–229.
Bae, J.S., Bhatia, S.K., 2006. High-pressure adsorption of methane and carbon dioxide on coal. Energy Fuels 20, 2599–2607.
Bruns, B., Littke, R., Gasparik, M., Wees, J.D., Nelskamp, S., 2016. Thermal evolution and shale gas potential estimation of the Wealden and Posidonia Shale in NW-Germany and the Netherlands: a 3D basin modelling study. Basin Res. 28, 2–33.
Busch, A., Gensterblum, Y., 2011. CBM and CO2-ECBM related sorption processes in coal: A review. Int. J. Coal Geol. 87, 49–71.
Bustin, R.M., Bustin, A., Ross, D., Chalmers, G., Murthy, V., Laxmi, C., Cui, X., 2009. Shale Gas Opportunities and Challenges. AAPG Annual Convention. San Antonio, Texas.
Cao, X.M., Yu, B.S., Li, X.T., Sun, M.D., Zhang, L., 2014. Reservoir characteristics and evaluation on logging of the Lower Cambrian gas shale in southeast Chongqing: a case study of Well Yuke 1 and Well Youke 1. Acta Pet. Sin. 35, 233–244 (in Chinese with English abstract).
Chalmers, G.R.L., Bustin, R.M., 2007. The organic matter distribution and methane capacity of the Lower Cretaceous strata of Northeastern British Columbia, Canada. Int. J. Coal Geol. 70, 223–239.
Chalmers, G.R.L., Bustin, R.M., 2008. Lower Cretaceous gas shales in northeastern British Columbia, part 1: geological controls on methane sorption capacity. Bull. Can. Pet. Geol. 56, 1–21.
Chareonsuppanimit, P., Mohammad, S.A., Robinson, J.R.L., Gasem, K.A.M., 2012. Highpressure adsorption of gases on shales: measurements and modeling. Int. J. Coal Geol. 95, 34–46.
Clarkson, C.R., Bustin, R.M., Levy, J.H., 1997. Application of the mono/multilayer and adsorption potential theories to coal methane adsorption isotherms at elevated temperature and pressure. Carbon 35, 1689–1705.
Curtis, J.B., 2002. Fractured shale-gas systems. AAPG Bull. 86, 1921–1938.
Cusack, C., Beeson, J., Stoneburner, D., Robertson, G., 2010. The discovery, reservoir attributes, and significance of the Hawkville Field and Eagle Ford Shale trend, Texas. Gulf Coast Assoc. Geol. Soc. Trans. 60, 165–179.
Dubinin, M.M., 1989. Fundamentals of the theory of adsorption in micropores of carbon adsorbents: characteristics of their adsorption properties and microporous structures. Carbon 27, 457–467.
Frantz, J.H., Williamson, J.R., Sawyer, W.K., et al. Evaluating Barnett Shale production performance – using an integrated approach. SPE Annual Technical Conference and Exhibition, 9–12 October 2005, Dallas, Texas. 10.2118/96917-MS. ISBN, 978-1-55563-150-5.
Gan, H., Zhang, H., Song, Y.T., 2015. Research on parameters of shale gas recoverability. Comp. Hyd. Reser. 8 (3), 22–26 (in Chinese with English abstract).
Gasparik, M., Betier, P., Gensterblum, Y., Ghanizadeh, A., Krooss, B.M., Littke, R., 2014a. Geological controls on the methane storage capacity in organic-rich shales. Int. J. Coal Geol. 123, 34–51.
Gasparik, M., Ghanizadeh, A., Bertier, P., Gensterblum, Y., Bouw, S., Krooss, B.M., 2012. Highpressure methane sorption isotherms of black shales from The Netherlands. Energy Fuel 26, 4995–5004.
Gasparik, M., Rexer, T.F.T., Aplin, A.C., Billemont, P., Weireld, G.D., Gensterblum, Y., Henry, M., Krooss, B.M., Liu, S.B., Ma, X.Z., Sakurovs, R., Song, Z.G., Staib, G., Thomas, K.M., Wang, S.B., Zhang, T.W., 2014b. First international inter-laboratory comparison of high-pressure CH4, CO2 and C2H6 sorption isotherms on carbonaceous shales. Int. J. Coal Geol. 132, 131–146.
Gensterblum, Y., Hemert, P.V., Billemont, P., Busch, A., Charriere, D., Li, D., Krooss, B.M., Weireld, G.D., Prinz, D., Wolf, K.H.A.A., 2009. European inter-laboratory comparison of high pressure CO_2 sorption isotherms. I: activated carbon. Carbon 47, 2958–2969.
Gensterblum, Y., Merkel, A., Busch, A., Krooss, B.M., Littke, R., 2014. Gas saturation and CO2 enhancement potential of coalbed methane reservoirs as a function of depth. AAPG Bull. 98, 395–420.
Gensterblum, Y., Merkel, A., Busch, A., Krooss, B.M., 2013. High-pressure CH4 and CO_2 sorption isotherms as a function of coal maturity and the influence of moisture. Int. J. Coal Geol. 118, 45–57.
Giovanni, O.D., Dorfler, W., Mazzotti, M., Morbidelli, M., 2001. Adsorption of supercritical carbon dioxide on silica. Langmiur 17, 4316–4321.
Gregg, S.J., Sing, K.S.W., 1982. Adsorption, Surface Area and Porosity, second ed. Academic Press, New York, p. 303.
Guo, T.L., Liu, R.B., 2013. Implications from marine shale gas exploration breakthrough in complicated structural area at high thermal stage: taking Longmaxi Formation in well JY1 as an example. Nat. Gas Geosci. 24, 643–651 (in Chinese with English abstract).
Guo, T.L., Zhang, H.R., 2014. Formation and enrichment mode of Jiashiba shale gas field, Sichuan Basin. Pet. Exp. Dev. 41, 28–36 (in Chinese with English abstract).
Guo, X.S., 2014. Rules of two-factor enrichment for marine shale gas in Southern China – understanding from the Longmaxi Formation shale gas in Sichuan Basin and its surrounding area. Acta Geol. Sin. 88, 1209–1218 (in Chinese with English abstract).
Guo, X.S., Hu, D.F., Wen, Z.D., Liu, R.S., 2014. Major factors controlling the accumulation and high productivity in marine shale gas in the lower Paleozoic of Sichuan Basin and its periphery: a case study of the Wufeng-Longmaxi Formation of Jiaoshiba area. Geol. China 41, 893–901 (in Chinese with English abstract).
Hammes, U., Hamlin, H.S., Ewing, T.E., 2011. Geologic analysis of the upper Jurassic Haynesville Shale in east Texas and west Louisiana. AAPG Bull. 95, 1645–1666.
Han, S.B., Zhang, L.C., Xing, Y.W., He, W., Xie, C., Jiang, S.L., Zhang, P., 2013. Shale gas accumulation conditions and resource potential of the Lower Silurian Longmaxi Formation in southeast Chongqing. J. China Coal Soc. 38, 168–173 (in Chinese with English abstract).

Hildenbrand, A., Krooss, B.M., Busch, A., Gaschnitz, R., 2006. Evolution of methane sorption capacity of coal seams as a function of burial history—A case study from the Campine Basin, NE Belgium. Int. J. Coal Geol. 66, 179–203.
Hill, R.J., Zhang, E., Katz, B.J., Tang, Y.C., 2007. Modeling of gas generation from the Barnett Shale, Fort Worth Basin, Texas. AAPG Bull. 91, 501–521.
Hu, D.F., Zhang, H.R., Ni, K., Yu, G.C., 2014. Main controlling factors for gas preservation conditions of marine shales in southeastern margins of the Sichuan Basin. Nat. Gas Ind. 34, 17–23 (in Chinese with English abstract).
Huang, J.L., Zou, C.N., Li, J.Z., Dong, D.Z., Wang, S.J., Wang, S.Q., Wang, Y.M., Li, D.H., 2012. Shale gas accumulation conditions and favorable zones of Silurian Longmaxi Formation in south Sichuan Basin, china. J. China Coal Soc. 37 (5), 782–787.
Jarvie, D.M., 2012. Shale resource systems for oil and gas: part 1-shale-gas resource systems. In: Breyer, J.A. (Ed.), Shale Reservoirs - Giant Resources for the 21st Century. AAPG Memoir 97, pp. 69–87.
Jarvie, D.M., Hill, R.J., Ruble, T.E., Pollastro, R.M., 2007. Unconventional shale-gas systems: the Mississippian Barnett shale of north-central texas as one model for thermogenic shale-gas assessment. AAPG Bull. 91, 475–499.
Ji, L.M., Zhang, T.W., Milliken, K.L., Qu, J.L., Zhang, X.L., 2012. Experimental investigation of main controls to methane adsorption in clay-rich rocks. Appl. Geochem 27, 2533–2545.
Ji, W., Song, Y., Jiang, Z., Wang, X., Bai, Y., Xing, J., 2014. Geological controls and estimation algorithms of lacustrine shale gas adsorption capacity: a case study of the Triassic strata in the southeastern Ordos Basin, China. Int. J. Coal Geol. 134–135, 61–73.
Krooss, R.M., Bergen, V.F., Gensterblum, Y., Siemons, N., Pagmier, H.J., David, P., 2002. High-pressure methane and carbon dioxide adsorption on dry and moisture-equilibrated Pennsylvanian coals. Int. J. Coal Geol. 51, 69–92.
Langmuir, I., 1918. The adsorption of gases on plane surfaces of glass, mica and platinum. J. Am. Chem. Soc. 40, 1361–1403.
Li, X.T., Shi, W.R., Guo, M.Y., Li, X., Zhao, H.Y., Chen, X., Ren, Y., Shi, Y.H., 2014. Characteristics of marine shale gas reservoirs in Jiashiba area of Fuling shale gas field. J. Oil Gas Technol. 36, 11–15 (in Chinese with English abstract).
Li, Y.F., Fan, T.L., Gao, Z.Q., Zhang, J.C., Wang, X.M., Zeng, W.T., Zhang, J.P., 2012. Sequence stratigraphy of Silurian black shale and its distribution in the southeast area of Chongqing. Nat. Gas Geosci. 23, 299–306 (in Chinese with English abtract).
Liang, C., Jiang, Z.X., Yang, Y.T., Wei, X.J., 2012. Characteristics of shale lithofacies and reservoir space of the Wufeng-Longmaxi Formation, Sichuan Basin. Pet. Exp. Dev. 39, 691–698 (in Chinese with English abstract).
Liu, H.L., Wang, H.Y., 2013. Ultra-low water saturation characteristics and the identification of over-pressured play fairways of marine shales in south China. Nat. Gas Ind. 33, 140–144 (in Chinese with English abstract).
Liu, R.B., 2015. Typical features of the first giant shale gas field in China. Nat. Gas Geosci. 26, 1488–1498 (in Chinese with English abstract).
Liu, S.G., Zeng, X.L., Huang, W.M., Ma, W.X., 2009. Basic characteristics of shale and continuous-discontinuous transition gas reservoirs in Sichuan Basin, China. J. Chengdu Univ. Technol. 36, 578–592 (in Chinese with English abstract).
Montgomery, S.L., Jarvie, D.M., Bowker, K.A., Ppllastro, R.M., 2005. Mississippian Barnett Shale, Fort Worth basin, north-central Texas: Gas-shale play with multi-trillion cubic foot potential. AAPG Bull. 89, 155–175.
Mosher, K., He, J., Liu, Y., Rupp, E., Wilcox, J., 2013. Molecular simulation of methane adsorption in micro- and mesoporous carbons with applications to coal and gas shale systems. Int. J. Coal Geol. 109–110, 36–44.
Mullen, J., 2010. Petrophysical characterization of the Eagle Ford Shale in South Texas. In: Canadian Unconventional Resources and International Petroleum Conference, 19–21 October 2010, Calgary, Alberta, Canada, ISBN 978-1-55563-312-7. http://dx.doi.org/10.2118/138145-MS.
Murata, K., El-Merraoui, M., Kaneko, K., 2001. A new determination method of absolute adsorption isotherm of supercritical gases under high pressure with a special relevance to density-functional theory study. J. Chem. Phys. 114, 4196–4205.
Murata, K., Miyawaki, J., Kaneko, K., 2002. A simple determination method of the absolute adsorbed amount for high pressure gas adsorption. Carbon 40, 425–428.
Nie, H.K., Bao, S.J., Gao, B., Bian, Z.K., Zhang, P.X., Wu, X.L., Ye, X., Chen, X.J., 2012. A study of shale gas preservation conditions for the Lower Paleozoic in Sichuan Basin and its periphery. Earth Sci. Front. 19, 280–294 (in Chinese with English abstract).
Nie, H.K., Tang, X., Bian, R.K., 2009. Controlling factors for shale gas accumulation and prediction of potential development area in shale gas reservoir of South China. Acta Pet. Sin. 30, 484–491 (in Chinese with English abstract).
Ottiger, S., Pini, R., Storti, G., Mazzotti, M., 2008. Competitive adsorption equilibria of CO_2 and CH_4 on a dry coal. Adsorption 14, 539–556.
Ottiger, S., Pini, R., Storti, G., Mazzotti, M., Bencini, R., Quattrocchi, F., Sardu, G., Deriu, G., 2006. Adsorption of pure carbon dioxide and methane on dry coal from the Sulcis Coal province (SW Sardinia, Italy). Environ. Prog. 25, 355–364.
Pini, R., Ottiger, S., Burlini, L., Storti, G., Mazzotti, M., 2010. Sorption of carbon dioxide, methane and nitrogen in dry coals at high pressure and moderate temperature. Int. J. Greenh. Gas Control 4, 90–101.
Pini, R., Ottiger, S., Rajendran, A., Storti, G., Mazzotti, M., 2006. Reliable measurement of near-critical adsorption by gravimetric method. Adsorption 12, 393–403.
Rexer, T.F.T., Benham, M.J., Aplin, A.C., Thomas, K.M., 2013. Methane adsorption on shale under simulated geological temperature and pressure conditions. Energy Fuels 27, 3099–3106.
Ross, D.J.K., Bustin, R.M., 2007. Impact of mass balance calculations on adsorption capacities in microporous shale gas reservoirs. Fuel 86, 2696–2706.
Ross, D.J.K., Bustin, R.M., 2008. Characterizing the shale gas resource potential of Devonian– Mississippian strata in the Western Canada sedimentary basin: application of an integrated formation evaluation. AAPG Bull. 92, 87–125.
Ross, D.J.K., Bustin, R.M., 2009. The importance of shale composition and pore structure upon gas storage potential of shale gas reservoirs. Mar. Pet. Geol. 26, 916–927.
Rouquerol, J., Avnir, D., Fairbridge, C.W., Everett, D.H., Haynes, J.H., Pernicone, N., Ramsay, J.D.F., Sing, K.S.W., Unger, K.K., 1994. Physical chemistry division Commission on colloid and surface Chemistry, subcommittee on characterization of porous solids: recommendations for the characterization of porous solids. Pure Appl. Chem. 66 (8), 1739–1758.
Sakurovs, R., Day, S., Weir, S., Duffy, G., 2007. Application of a modified Dubinin-Radushkevich equation to adsorption of gases by coals under supercritical conditions. Energy Fuels 21, 992–997.
Shi, W.R., Guo, M.Y., Zhang, J.P., Feng, A.G., Zhao, H.Y., Ye, Y.G., Shi, Y.H., 2015. Experimental study on the adsorption and desorption of shale gas. Mud Log. Eng. 26, 9–12 (in Chinese with English abstract).
Sudibandriyo, M., Pan, Z.J., Fitzgerald, J.E., Robinson, R.L., Gasem, K.A.M., 2003. Adsorption of methane, nitrogen, carbon dioxide, and their binary mixtures on dry activated carbon at 318.2 K and pressures up to 13.6 MPa. Langmuir 19, 5323–5331.
Sun, M.D., Yu, B.S., Li, J., Cao, X.M., Xia, W., 2014. Features and major controlling factors of Longmaxi shale reservoir in Southeastern Chongqing. Spe Oil Gas Res. 21, 63–66 (in Chinese with English abstract).
Tan, L.Y., Xu, Y., Li, D.H., Cheng, L.J., Zeng, X.L., 2015. Geological condition of shale gas accumulation and favorable area prediction for the Wufeng-Longmaxi Formation in Southeastern Chongqing. Acta Geol. Sin. 89, 1308–1317 (in Chinese with English abstract).
Tian, H., Pan, L., Xiao, X.M., Wilkins, R.W.T., Meng, Z.P., Huang, B.J., 2013. A preliminary study on the pore characterization of Lower Silurian black shales in the Chuandong Thrust Fold Belt, southwestern China using low pressure N_2 adsorption and FE-SEM methods. Mar. Pet. Geol. 48, 8–19.
Tian, H., Pan, L., Zhang, T.W., Xiao, X.M., Meng, Z.P., Huang, B.J., 2015. Pore characterization of organic-rich lower Cambrian shales in Qiannan depression of Guizhou province, Southwestern China. Mar. Pet. Geol. 62, 28–43.
Wang, F.Y., Guan, J., Feng, W.P., Bao, L.Y., 2013a. Evolution of overmature marine shale porosity and implication to the free gas volume. Pet. Exp. Dev. 40 (6), 819–824.
Wang, S.B., Song, Z.G., Cao, T.T., Song, X., 2013b. The methane sorption capacity of Paleozoic shales from the Sichuan Basin, China. Mar. Pet. Geol. 44, 112–119.
Wang, Y.F., 2012. Study on the natural gas generation through basin modeling in eastern Sichuan Basin. Grad. Uni. Chin. Acad. Sci. 15–40 (in Chinese with English abstract).
Wang, Z.G., 2014. Practice and cognition of shale gas horizontal well fracturing stimulation in Jiaoshiba of Fuling area. Oil Gas Geol. 35, 425–430 (in Chinese with English abstract).
Wei, Z.H., Wei, X.F., 2014. Comparison of gas-bearing property between different pore types of shale: a case from the Upper Ordovician Wufeng and Longmaxi Fms in the Jiaoshiba area, Sichuan Basin. Nat. Gas Ind. 34, 37–41 (in Chinese with English abstract).
Weniger, P., Kalkreuth, W., Busch, A., Krooss, B.M., 2010. High-pressure methane and carbon dioxide sorption on coal and shale samples from the Parana Basin, Brazil. Int. J. Coal Geol. 84, 190–205.
White, C.M., Smith, D.H., Jones, K.L., Goodman, A.L., Jikich, S.A., LaCount, R.B., DuBose, S.B., Ozdermir, E., Morsi, B.I., Schroeder, K.T., 2005. Sequestration of carbon dioxide in coal with enhanced coalbed methane reservoirs – a review. Energy Fuels 19, 659–724.
Wu, J.S., Yu, B.S., Li, Y.X., 2012. Adsorption capacity of shale gas and controlling factors from the well Yuye 1 at the Southeast of Chongqing. J. South. Pet. Univ. 34, 40–48 (in Chinese with English abstract).
Xie, C., Zhang, J.C., Li, Y.X., Wang, X.H., 2013. Characteristics and gas content of the lower Cambrian dark shale in Well Yuke 1, Southeast Chongqing. Oil Gas Geol. 34, 11–15 (in Chinese with English abstract).
Xing, Y.W., Zhang, J.C., Feng, H.Q., Zheng, F.J., Bai, X.B., 2014. Accumulation conditions and resource potential of Lower Cambrian shale gas in southeast Chongqing. J. North. Pet. Univ. 38, 66–74 (in Chinese with English abstract).
Yang, H.C., Mao, G.Y., Song, Q.C., Ji, Z.J., Liu, F.Z., 2014. Large scale fracturing technology of well Pengye HF-1 shale gas. J. South. Pet. Univ. 36, 117–122 (in Chinese with English abstract.
Yuan, Y.S., Ma, Y.S., Hu, S.B., Guo, T.L., Fu, X.Y., 2006. Present-day geothermal characteristics in South China. Chin. J. Geophys. 49, 1118–1126 (in Chinese with English abstract).
Zhai, Y.J., 2014. Shale gas accumulation conditions and favourable areas forecast of Lower Silurian in East Chongqing. China Univ. Geosc. Beijing 15–25 (in Chinese with English abstract).
Zhang, J.C., Lin, L.M., Li, Y.X., Jiang, S.L., Liu, J.X., Jiang, W.L., Tang, X., Han, S.B., 2012a. The method of shale gas assessment: probability volume method. Earth Sci. Front. 19, 184–191.
Zhang, J.C., Nie, H.K., Xu, B., Jiang, S.L., Zhang, P.X., Wang, Z.Y., 2008. Geological condition of shale gas accumulation in Sichuan Basin. Nat. Gas Ind. 28, 151–156 (in Chinese with English abstract).
Zhang, Q., Liu, H.L., Bai, W.H., Lin, W., 2013. Shale gas content and its main

controlling factors in Longmaxi shales in southeastern Chongqing. Nat. Gas Ind. 33 (5), 35–39 (in Chinese with English abstract).
Zhang, T.W., Ellis, G.S., Ruppel, S.C., Milliken, K., Yang, R.S., 2012b. Effect of organic-matter type and thermal maturity on methane adsorption in shale-gas systems. Org. Geochem. 47, 120–131.
Zhou, D.H., Jiao, F.Z., Jia, C.G., Jiang, T.X., Li, Z.X., 2014a. Large-scale multi-stage hydraulic fracturing technology for shale gas horizontal well JY1HF. Pet. Drill. Tech. 42 (1), 75–80 (in Chinese with English abstract).
Zhou, Q., 2014. Modelling gas generation and reserve potentials of lower Paleozoic shales in the middle and southern areas of Sichuan Basin. Univ. Chin. Acad. Sci. 64–89 (in Chinese with English abstract).
Zhou, Q., Xiao, X.M., Tian, H., Pan, L., 2014b. Modeling free gas content of the Lower Paleozoic shales in the Weiyuan area of the Sichuan Basin, China. Mar. Pet. Geol. 56, 87–96.
Zhou, X.H., 2013. Drilling & completion techniques used in shale gas horizontal wells in Jiaoshiba block of Fuling area. Pet. Drill. Tech. 41, 26–30 (in Chinese with English abstract).